Physics Letters B 299 (1993) 385–393
North-Holland

PHYSICS LETTERS B

Observation of deep inelastic scattering at low x

H1 Collaboration

T. Ahmed[a], V. Andreev[b], B. Andrieu[c], M. Arpagaus[d], A. Babaev[e], H. Bärwolff[f], J. Bán[g], P. Baranov[b], E. Barrelet[h], W. Bartel[i], U. Bassler[h], G.A. Beck[j], H.P. Beck[k], H.-J. Behrend[i], A. Belousov[b], Ch. Berger[ℓ], H. Bergstein[ℓ], G. Bernardi[h], R. Bernet[d], U. Berthon[c], G. Bertrand-Coremans[m], M. Besançon[n], P. Biddulph[o], E. Binder[i], J.C. Bizot[p], V. Blobel[q], K. Borras[r], P.C. Bosetti[s], V. Boudry[c], C. Bourdarios[p], F. Brasse[i], U. Braun[s], W. Braunschweig[ℓ], V. Brisson[p], D. Bruncko[g], J. Bürger[i], F.W. Büsser[q], A. Buniatian[i,1], S. Burke[j], G. Buschhorn[t], A.J. Campbell[u], T. Carli[c], F. Charles[h], D. Clarke[v], A.B. Clegg[w], M. Colombo[r], J.A. Coughlan[v], A. Courau[p], Ch. Coutures[n], G. Cozzika[n], L. Criegee[i], J. Cvach[c], J.B. Dainton[j], M. Danilov[e], A.W.E. Dann[o], W.D. Dau[x], M. David[n], E. Deffur[i], B. Delcourt[p], L. Del Buono[h], M. Devel[p], A. De Roeck[i], P. Dingus[c], C. Dollfus[k], J.D. Dowell[a], H.B. Dreis[s], A. Drescher[r], J. Duboc[h], D. Düllmann[q], O. Dünger[q], H. Duhm[y], M. Eberle[y], J. Ebert[z], T.R. Ebert[j], G. Eckerlin[i], V. Efremenko[e], S. Egli[k], S. Eichenberger[k], R. Eichler[d], F. Eisele[i], E. Eisenhandler[aa], N.N. Ellis[a], R.J. Ellison[o], E. Elsen[i], M. Erdmann[i], E. Evrard[m], L. Favart[m], A. Fedotov[e], D. Feeken[q], R. Felst[i], J. Feltesse[n], Y. Feng[h], I.F. Fensome[a], J. Ferencei[i], F. Ferrarotto[ab], W. Flauger[i,2], M. Fleischer[i], P.S. Flower[v], G. Flügge[s], A. Fomenko[b], B. Fominykh[e], M. Forbush[ac], J. Formánek[ad], J.M. Foster[o], G. Franke[i], E. Fretwurst[y], P. Fuhrmann[ℓ], E. Gabathuler[j], K. Gamerdinger[t], J. Garvey[a], J. Gayler[i], A. Gellrich[q], M. Gennis[i], U. Gensch[f], H. Genzel[ℓ], R. Gerhards[i], D. Gillespie[j], L. Godfrey[ac], U. Goerlach[i], L. Goerlich[ae], M. Goldberg[h], A.M. Goodall[j], I. Gorelov[e], P. Goritchev[e], C. Grab[d], H. Grässler[s], R. Grässler[s], T. Greenshaw[j], H. Greif[t], G. Grindhammer[t], C. Gruber[x], J. Haack[f], D. Haidt[i], L. Hajduk[ae], O. Hamon[h], D. Handschuh[i], E.M. Hanlon[w], M. Hapke[i], J. Harjes[q], P. Hartz[r], R. Haydar[p], W.J. Haynes[v], J. Heatherington[aa], V. Hedberg[af], R. Hedgecock[v], G. Heinzelmann[q], R.C.W. Henderson[w], H. Henschel[f], R. Herma[ℓ], I. Herynek[ag], W. Hildesheim[h], P. Hill[i], C.D. Hilton[o], J. Hladký[ag], K.C. Hoeger[o], Ph. Huet[m], H. Hufnagel[r], N. Huot[h], M. Ibbotson[o], M.A. Jabiol[n], A. Jacholkowska[p], C. Jacobsson[af], M. Jaffre[p], L. Jönsson[af], K. Johannsen[q], D.P. Johnson[m], L. Johnson[w], H. Jung[s], P.I.P. Kalmus[aa], S. Kasarian[i], R. Kaschowitz[s], P. Kasselmann[y], U. Kathage[x], H.H. Kaufmann[f], I.R. Kenyon[a], S. Kermiche[p], C. Kiesling[t], M. Klein[f], C. Kleinwort[q], G. Knies[i], T. Köhler[ℓ], H. Kolanoski[r], F. Kole[ac], S.D. Kolya[o], V. Korbel[i], M. Korn[r], P. Kostka[f], S.K. Kotelnikov[b], M.W. Krasny[ae,n], H. Krehbiel[i], D. Krücker[s], U. Krüger[i], J.P. Kubenka[t], H. Küster[i], M. Kuhlen[t], T. Kurça[g], J. Kurzhöfer[r], B. Kuznik[z], R. Lander[ac], M.P.J. Landon[aa], R. Langkau[y], P. Lanius[t], J.F. Laporte[n], A. Lebedev[b], A. Leuschner[i], C. Leverenz[i], D. Levin[i], S. Levonian[i,b], Ch. Ley[s], A. Lindner[r], G. Lindström[y], P. Loch[i], H. Lohmander[af], G.C. Lopez[aa], D. Lüers[t,2], N. Magnussen[z], E. Malinovski[b], S. Mani[ac], P. Marage[m], J. Marks[u], R. Marshall[o], J. Martens[z], R. Martin[j], H.-U. Martyn[ℓ], J. Martyniak[ae], S. Masson[s], A. Mavroidis[aa], S.J. Maxfield[j], S.J. McMahon[j], A. Mehta[o], K. Meier[i], T. Merz[i], C.A. Meyer[k], H. Meyer[z], J. Meyer[i], S. Mikocki[ae,p], V. Milone[ab], E. Monnier[h], F. Moreau[c], J. Moreels[m], J.V. Morris[v], J.M. Morton[j], K. Müller[k], P. Murín[g], S.A. Murray[o], V. Nagovizin[e], B. Naroska[q], Th. Naumann[f], D. Newton[w], H.K. Nguyen[h], F. Niebergall[q],

R. Nisius[ℓ], G. Nowak[ae], G.W. Noyes[a], M. Nyberg[af], H. Oberlack[t], U. Obrock[r], J.E. Olsson[i], S. Orenstein[c], F. Ould-Saada[q], C. Pascaud[p], G.D. Patel[j], E. Peppel[i], S. Peters[t], H.T. Phillips[a], J.P. Phillips[o], Ch. Pichler[y], W. Pilgram[s], D. Pitzl[d], R. Prosi[i], F. Raupach[ℓ], K. Rauschnabel[r], P. Reimer[ag], P. Ribarics[t], V. Riech[y], J. Riedlberger[d], M. Rietz[s], S.M. Robertson[a], P. Robmann[k], R. Roosen[m], A. Rostovtsev[e], C. Royon[n], M. Rudowicz[t], M. Ruffer[y], S. Rusakov[b], K. Rybicki[ae], E. Ryseck[f], J. Sacton[m], N. Sahlmann[s], E. Sanchez[t], D.P.C. Sankey[v], M. Savitsky[i], P. Schacht[t], P. Schleper[ℓ], W. von Schlippe[aa], C. Schmidt[i], D. Schmidt[z], W. Schmitz[s], V. Schröder[i], M. Schulz[i], A. Schwind[f], W. Scobel[y], U. Seehausen[q], R. Sell[i], M. Seman[g], A. Semenov[e], V. Shekelyan[e], I. Sheviakov[b], H. Shooshtari[ab], G. Siegmon[x], U. Siewert[x], Y. Sirois[c], I.O. Skillicorn[u], P. Smirnov[b], J.R. Smith[ac], L. Smolik[i], Y. Soloviev[b], H. Spitzer[q], P. Staroba[ag], M. Steenbock[q], P. Steffen[i], R. Steinberg[s], H. Steiner[h], B. Stella[ab], K. Stephens[o], J. Stier[i], J. Strachota[i], U. Straumann[k], W. Struczinski[s], J.P. Sutton[o], R.E. Taylor[ah,p], G. Thompson[aa], R.J. Thompson[o], I. Tichomirov[e], C. Trenkel[x], P. Truöl[k], V. Tchernyshov[e], J. Turnau[ae], J. Tutas[ℓ], L. Urban[t], A. Usik[b], S. Valkar[ad], A. Valkarova[ad], C. Vallee[h], P. Van Esch[m], A. Vartapetian[i,1], Y. Vazdik[b], M. Vecko[ag], P. Verrecchia[n], R. Vick[q], G. Villet[n], E. Vogel[ℓ], K. Wacker[r], I.W. Walker[w], A. Walther[r], G. Weber[q], D. Wegener[r], A. Wegner[i], H.P. Wellisch[t], S. Willard[ac], M. Winde[f], G.-G. Winter[i], Th. Wolff[d], L.A. Womersley[j], A.E. Wright[o], N. Wulff[i], T.P. Yiou[h], J. Záçek[p,ad], P. Závada[ag], C. Zeitnitz[y], H. Ziaeepour[p], M. Zimmer[i], W. Zimmermann[i] and F. Zomer[p]

[a] *School of Physics and Space Research, University of Birmingham, Birmingham B15 2TT, UK*[3]
[b] *Lebedev Physical Institute, 117 924 Moscow, Russian Federation*
[c] *LPNHE, Ecole Polytechnique, IN2P3-CNRS, F-91128 Palaiseau Cedex, France*
[d] *Institut für Mittelenergiephysik, ETH, Zürich, CH-5232 Villigen, Switzerland*[4]
[e] *Institute for Theoretical and Experimental Physics, 117 259 Moscow, Russian Federation*
[f] *DESY, Institut für Hochenergiephysik, O-1615 Zeuthen, FRG*[5]
[g] *Institute of Experimental Physics, Slovak Academy of Sciences, CS-043 53 Kosice, Slovak Republic*
[h] *LPNHE, Universités Paris VI and VII, IN2P3-CNRS, F-75252 Paris Cedex 05, France*
[i] *DESY, Hamburg, W-2000 Hamburg 52, FRG*[5]
[j] *Department of Physics, University of Liverpool, Liverpool L69 3BX, UK*[3]
[k] *Physik-Institut der Universität Zürich, CH-8001 Zurich, Switzerland*[4]
[ℓ] *I. Physikalisches Institut der RWTH, W-5100 Aachen, FRG*[5]
[m] *Inter-University Institute for High Energies ULB-VUB, B-1050 Brussels, Belgium*[6]
[n] *DAPNIA, Centre d'Etudes de Saclay, F-91191 Gif-sur-Yvette Cedex, France*
[o] *Physics Department, University of Manchester, Manchester M13 9PL, UK*[3]
[p] *LAL, Université de Paris-Sud, IN2P3-CNRS, F-91405 Orsay Cedex, France*
[q] *II. Institut für Experimentalphysik, Universität Hamburg, W-2000 Hamburg 50, FRG*[5]
[r] *Institut für Physik, Universität Dortmund, W-4600 Dortmund 50, FRG*[5]
[s] *III. Physikalisches Institut der RWTH, W-5100 Aachen, FRG*[5]
[t] *Max-Planck-Institut für Physik, W-8000 Munich 40, FRG*[5]
[u] *Department of Physics and Astronomy, University of Glasgow, Glasgow G12 8QQ, UK*[3]
[v] *Rutherford Appleton Laboratory, Chilton, Didcot OX11 0QX, UK*[3]
[w] *School of Physics and Materials, University of Lancaster, Lancaster LA1 4YB, UK*[3]
[x] *Institut für Reine und Angewandte Kernphysik, Universität Kiel, W-2300 Kiel 1, FRG*[5]
[y] *I. Institut für Experimentalphysik, Universität Hamburg, W-2000 Hamburg, FRG*[5]
[z] *Fachbereich Physik, Bergische Universität Gesamthochschule Wuppertal, W-5600 Wuppertal 1, FRG*[5]
[aa] *Queen Mary and Westfield College, London E1 4NS, UK*[3]
[ab] *INFN Roma and Dipartimento di Fisica, Università "La Sapienzia", I-00185 Rome, Italy*
[ac] *Physics Department and IIRPA, University of California, Davis, CA, USA*[7]
[ad] *Nuclear Center, Charles University, CS-180 00 Prague 8, Czech Republic*
[ae] *Institute for Nuclear Physics, Cracow, Poland*
[af] *Physics Department, University of Lund, S-223 62 Lund, Sweden*[8]

[ag] *Institute of Physics, Czechoslovak Academy of Sciences, CS-180 40 Prague, Czech Republic*
[ah] *Stanford Linear Accelerator Center, Stanford, CA 94309, USA*

Received 23 November 1992

Measurements of the scattered electron energy spectrum and the differential cross sections $d\sigma/d\log(x)$ and $d\sigma/dQ^2$ for inclusive neutral current deep inelastic electron-proton scattering are presented. The data were obtained with the H1 detector at HERA during its first running period in which 26.7 GeV electrons collided with 820 GeV protons. The data correspond to an integrated luminosity of 1.3 nb^{-1} and allow the first studies of the structure of the proton at values of x down to 10^{-4} for $Q^2 > 5$ GeV^2.

1. Introduction

Since the discovery of partons more than 20 years ago [1], deep inelastic lepton scattering experiments [2,3] have provided important information on the structure of the proton and on the nature of the interactions between leptons and quarks. The electron–proton collider HERA allows the extension of this line of research into as yet unexplored kinematic regions.

This paper describes the analysis of data taken with the H1 detector [4,5] in July of 1992, HERA's first running period. Both the H1 and ZEUS experiments have presented preliminary results from this period [4,6].

The kinematics of the inclusive deep inelastic scattering (DIS) process $ep \to eX$ is determined by two independent variables, conventionally chosen to be two of x, y and Q^2. These variables may be measured using information from either the scattered lepton or the hadronic system or both. The polar angle θ_e of the scattered electron is measured relative to the proton beam direction, termed the forward direction in the following. The angle, θ_e, and the energy of the scattered lepton, E'_e, determine the above variables through the relations

$$Q^2 = 4E_eE'_e\cos^2(\tfrac{1}{2}\theta_e),$$
$$y = 1 - (E'_e/E_e)\sin^2(\tfrac{1}{2}\theta_e),$$
$$x = Q^2/sy, \tag{1}$$

where the centre of mass energy squared $s = 4E_eE_p = 87\,600$ GeV^2, and E_e and E_p are the energies of the incoming electron and proton, respectively. Due to the large centre of mass energy, x values down to $\sim 10^{-4}$ can be studied in the deep inelastic regime. A salient feature of the kinematics is a peak in the scattered electron energy spectrum at the beam energy E_e for electrons scattered into the backward region $\theta_e > 150°$. This peak, termed the kinematic peak in the following, is of particular interest for calibration purposes. The outgoing hadrons are used for a complementary determination of y using the relation [7]

$$y_h = \sum_{\text{hadrons}} \frac{E_h - p_{z,h}}{2E_e}, \tag{2}$$

where the E_h are the energies of the hadrons and the p_z their momenta in the z or proton beam direction.

At HERA the electroweak interaction rate is orders of magnitude smaller than the background rate caused by strong interactions of beam protons with either the residual gas in the beampipe or with the material of the beampipe itself. Moreover, at low scattered electron energies, the background rate due to photoproduction events is much larger than the rate of deep inelastic events. The identification of the deep inelastic events is discussed in detail in the following. The data sample is used to derive a first measurement of the neutral current cross section in the new kinematic range.

1 Visitor from Yerevan Physical Institute, 375036 Yerevan, Armenia.
2 Deceased.
3 Supported by the UK Science and Engineering Research Council.
4 Supported by the Swiss National Science Foundation.
5 Supported by the Bundesministerium für Forschung und Technologie, FRG.
6 Supported by IISN-IIKW, NATO CRG-890478.
7 Supported in part by US DOE grant DE F603 91ER40674.
8 Supported by the Swedish Natural Science Research Council.

2. The H1 detector

Fig. 1 shows a deep inelastic scattering event at $x = 0.002$ and $Q^2 = 17\ \mathrm{GeV}^2$ observed in the H1 detector. Most of the detector components important for this analysis are visible. These are

- The tracker: the central tracking detector consists of two large jet drift chamber modules, two z drift chambers and two multiwire proportional chambers for triggering. Its angular acceptance is 15°–170°. The forward tracking detector accepts tracks between 7° and 25°. It consists of three modules of drift and multiwire proportional chambers. The backward multiwire proportional chamber (BPC) has four wire planes and an angular acceptance of 155°–175°. A superconducting coil provides a uniform magnetic field of 1.2 T in the tracking region.
- The calorimeters: the backward electromagnetic calorimeter (BEMC) is made of 88 lead/scintillator sandwich stacks, each with a depth of 22 radiation lengths, corresponding to about 0.7 interaction lengths, and transverse dimensions of $16 \times 16\ \mathrm{cm}^2$. The liquid argon calorimeter consists of an electromagnetic section with lead absorber (20–30 radiation lengths) and a hadronic section with steel absorber. The total depth of the calorimeter varies between 4.5 and 8 interaction lengths.
- The time of flight (TOF) system, located behind the backward calorimeter, consists of two scintillator planes, each with a time resolution of about 3 ns, and enables the separation of genuine ep events from proton beam–wall and beam–gas interactions upstream of the detector at the trigger level.
- The luminosity detector system described in ref. [8], not visible in fig. 1, is designed to detect the e–γ coincidence from the reaction $e + p \to e + \gamma + p$. The electron tagger is located 33 m from the interaction region in the backward or $-z$ direction and detects electrons scattered through angles less than 5 mrad with respect to the electron beam direction. The photon tagger is located at $z = -103$ m. Both detectors are TlCl/TlBr crystal calorimeters.

At low values of Q^2 the scattered electron deposits its energy in the backward electromagnetic calorimeter. The scattering angle is determined using the backward proportional chamber and the reconstructed event vertex and, at smaller θ_e, the drift chambers. The angles and energies of hadronic final state parti-

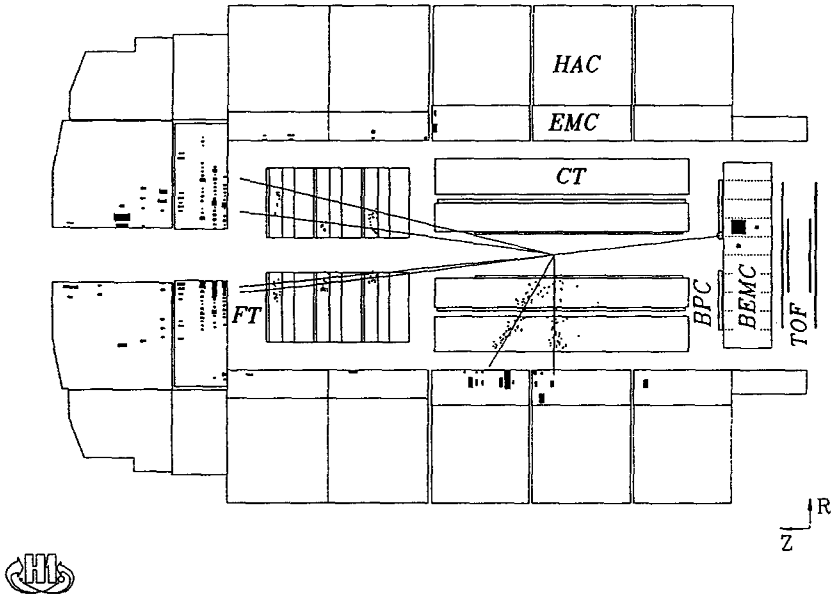

Fig. 1. A deep inelastic scattering event at $x = 0.002$ and $Q^2 = 17\ \mathrm{GeV}^2$, observed in the H1 detector. The detector components shown are the electromagnetic (EMC), hadronic (HAC) and backward electromagnetic (BEMC) calorimeters, forward (FT) and central (CT) trackers, backward proportional chamber (BPC), and scintillator hodoscope (TOF).

cles are measured with the central and forward tracking systems and with the liquid argon and backward calorimeters. The analysis in this paper is restricted to electrons detected in the backward calorimeter.

3. Calibration and resolution

The energy resolution of the BEMC due to sampling fluctuations is $10\%/\sqrt{E}$, as has been determined in test beam studies [9]. The average noise per stack was measured to be 150 MeV which implies that the noise contribution to the measurement of a typical scattered electron shower is about 450 MeV. The measured energy has to be corrected for energy loss in the material in front of the BEMC (about 1 X_o), losses in the wavelength shifter regions between the stacks and for leakage. Monte Carlo simulations showed that all these effects combined give a 2.7% energy correction on average with a fluctuation of $\pm 1.2\%$ due to inhomogeneities. The energy resolution is further affected by stack to stack intercalibration uncertainties which are estimated to be 3.7%. From these considerations the following energy resolution was derived: $\sigma_E/E = \sigma_{\text{noise}}/E \oplus \sigma_{\text{sampling}}/\sqrt{E} \oplus \sigma_{\text{const}}$, where $\sigma_{\text{noise}} = 0.45$ GeV, $\sigma_{\text{sampling}} = 0.1$ GeV$^{1/2}$, $\sigma_{\text{const}} = 0.04$ and E is measured in GeV. This results in a width of the simulated kinematic peak, due to the intrinsic width and detector effects, of about 2.2 GeV which agrees with the observed width.

In the kinematic peak region ($E > 22$ GeV) a χ^2 comparison of the observed energy spectrum with the Monte Carlo prediction was used to determine the overall BEMC energy calibration. An additional check was performed by deriving the scattered electron energy from the angles θ_e of the electron and θ_h of the momentum vector of the hadronic system. The energy calibration has an uncertainty of 2%. For the determination of y_h from the hadronic final state a combination of well measured tracks in the central region with energy deposits in the calorimeter was used. The calibration of the liquid argon calorimeter is presently known to 2% for the electromagnetic and to 7% for the hadronic energies [10].

For angles between 174° and about 170°, the electron scattering angle θ_e is determined by the vertex of the event and the reconstructed hit in the BPC. Events at low y which contribute to the energy distribution in the kinematic peak may leave no track in the detector. These are included in the electron energy spectrum but not in the Q^2 and x distributions. For smaller angles ($< 170°$), θ_e can be reconstructed from tracks in the central chambers. The angular resolution $\delta\theta_e$ depends only weakly on θ_e and is about 6 mrad for interactions with a reconstructed vertex.

The four-momentum transfer squared is determined from the energy and angle of the scattered electron. With the exception of extremely large polar angles, the resolution $\delta Q^2/Q^2$ is dominated by the electron energy resolution and is about 6%. An alternative calculation of Q^2 using the two scattering angles θ_e and θ_h has a similar resolution, essentially independent of Q^2, and was used as a consistency check. For the determination of $x = Q^2/sy$ it is advantageous to combine leptonic and hadronic measurements of y. The resolution $\delta y_e/y_e$ varies like $1/y$ and is 5% at $y = 0.6$ but deteriorates to 30% for $y = 0.1$. The y_h resolution is better than about 30% for $y_h > 0.025$. Hence, for $y_e < 0.1$, y_h was used in preference to y_e. The resulting x resolution varies between 15% at $x = 10^{-4}$ and 35% at $x = 10^{-2}$. For $x > 10^{-2}$ and small Q^2 hadrons are lost in the forward beam pipe region and x measurements are subject to systematic shifts. This will require detailed study in future high statistics analyses.

4. Event selection and background

The data presented here correspond to a total integrated luminosity of 1.3 nb^{-1}, which is known to a precision of 7%. The trigger pertinent to this analysis required that a local energy deposit, or cluster, of more than 4 GeV be identified in the BEMC. Events were rejected if signals in both TOF planes were compatible with particles produced in upstream proton background interactions. The acceptance of this trigger increased from 90% to 99% for electron energies between 5 and 10 GeV and was larger than 99% for electron energies above this. The total number of such triggers recorded was about 6×10^4.

Deep inelastic scattering event candidates were identified using the following criteria:

– A cluster of more than 6 GeV was required in the backward calorimeter in association with at least one hit in the adjacent BPC. The radial separation of the centre of gravity of the cluster and the BPC hit was required to be less than 15 cm. Furthermore, the cluster centre of gravity had to lie outside the range $|x|$ or $|y| > 16$ cm around the beam axis.

- For events with a BEMC cluster energy below the kinematic peak region (E_e <22 GeV) it was required that at least one track in the central tracker originate from the transverse beam position. The z coordinate of the vertex had to be within ± 50 cm of the nominal interaction point, compatible with the width of the z-vertex distribution of 40 cm (FWHM).

- Out of time proton beam background was further suppressed by restrictive cuts on the signals from the individual TOF scintillator planes.

The resulting sample of 219 events was scanned for remaining beam background and cosmic events, which were removed. The sample of DIS candidates surviving all selection criteria comprised 182 events. In this sample six events were observed with a clear electron tagger signal in coincidence with an energy deposit in the BEMC of less than 10 GeV. These are events where the scattered electron disappears in the beampipe, but hadrons and photons produced in the backward region simulate an electron signal in the BEMC. This implies that the DIS sample contained about 20–40 photoproduction events at this stage of the selection procedure. Further evidence for the presence of this background was provided by a comparison of the hadron and the electron y measurements, shown in fig. 2a. A clear correlation between y_e and y_h is evident in the region in which the y_e resolution is good, $y_e > 0.1$; yet, independent of y_h, there is also an accumulation of events at high y_e, i.e., low electron energies. Fig. 2b shows a Monte Carlo calculation of y_h and y_e, based on the vector dominance model (VDM) [11] for photoproduction. As in the data an accumulation of events at high y_e is seen. Detailed Monte Carlo studies of the photoproduction background using various event generators [11,12], and resolution considerations, led us to reject events if $y_h < \frac{1}{2}y_e$, for $y_e > 0.6$. The resulting event sample contained 148 events, none of which had a signal in the electron tagger. The remaining photoproduction contamination could be as much as 50% for $E'_e < 10$ GeV but is estimated to be less than 20% for $10 < E'_e < 14$ GeV. For $E'_e > 14$ GeV the photoproduction contamination is negligible. Note that $y = 0.6$ corresponds roughly to $E'_e = 10$ GeV. The lowest x event in this sample has

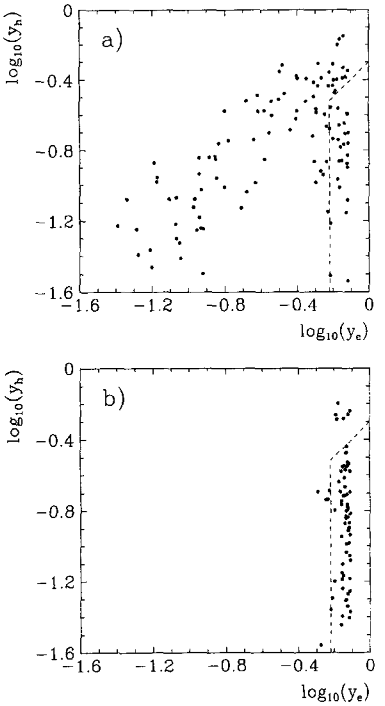

Fig. 2. Distribution of $\log_{10}(y_e)$ versus $\log_{10}(y_h)$ for (a) DIS candidates and (b) simulated background events based on the VDM photoproduction event generator [11]. The simulated statistics corresponds to 2.5 nb^{-1}. The dashed lines mark the region of the y cut which was used to remove photoproduction background.

$x = 6 \times 10^{-5}$ at $Q^2 = 4$ GeV^2 while the largest [#1] Q^2 event has a $Q^2 = 82$ GeV^2 at $x = 4 \times 10^{-3}$.

The contamination of the DIS sample with proton and electron beam induced background was estimated to be less than 5% for $E'_e > 10$ GeV, based on studies of the multiplicity of identified low momentum protons and of studies of e and p bunches which have no partner to collide with. Another potential background comes from event pile-up. Due to the high HERA bunch crossing rate of 10 MHz the detector information for an interaction can be distorted by signals resulting from a collision in adjacent bunch crossings.

[#1] In the same data taking period five neutral currents events were detected in the liquid argon calorimeter with $Q^2 > 100$ GeV^2.

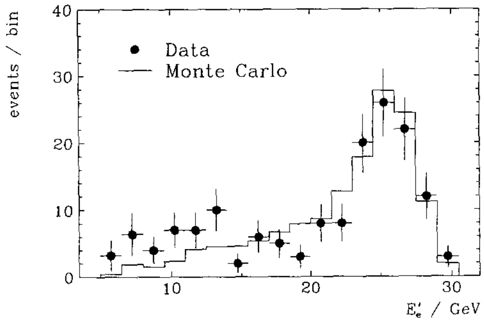

Fig. 3. Electron energy spectrum of the DIS events compared with a Monte Carlo simulation [13,14] of the H1 detector using the parametrization MRSD0 [15]. The simulated spectrum is normalized to the measured integrated luminosity of 1.3 nb^{-1}.

The number of events affected by pile-up was estimated to be less than 1%.

The energy spectrum of the scattered electron for the accepted data sample is shown in fig. 3. The expected peak of the distribution at $E'_e = E_e$ is clearly visible. The measured spectrum is compared with a Monte Carlo calculation including a full simulation of the H1 detector. The events have been generated using HERACLES 3.1 [13] for the electroweak interaction, which includes first order radiative corrections, followed by LEPTO 5.2 [14] for the simulation of QCD processes. We chose to represent the parton distributions using the MRSD0 parametrization described in ref. [15]. The simulated distribution in fig. 3 was normalized to the measured luminosity. Between 12 and 30 GeV the spectra agree well with a χ^2 of 7.2 for eight degrees of freedom. The data contain more events in the low energy region than is predicted by the Monte Carlo calculation. This may be due to remaining photoproduction contamination and a low x behaviour of the proton structure functions which is different from that of the MRSD0 parametrization.

5. Differential cross sections

In the Born approximation the deep inelastic scattering cross section at low Q^2 is determined by the two structure functions F_2 and $2xF_1 = F_2/(1+R)$:

$$\frac{d^2\sigma}{dx\,dQ^2} = \frac{2\pi\alpha^2}{Q^4 x}\left(2(1-y) + \frac{y^2}{1+R}\right) F_2(x,Q^2) . \qquad (3)$$

In order to reduce sensitivity to the photoproduction background and to the effects of radiative corrections [16,17] the cross section analysis was limited to $y < 0.6$ [#2]. As discussed above, a lower y limit was set at $y = 0.025$, ensuring that the y resolution was always better than 30%. In addition it was demanded that $Q^2 > 5$ GeV^2, $\theta_e < 174°$ and that the ep interaction vertex be reconstructed, thus reducing the sample to 72 events. The rejected events are primarily at high E'_e where for kinematic reasons hadrons are produced with small angles.

The observed distributions were normalized to the measured luminosity and converted into differential cross sections by correcting for the acceptance and finite bin size effects. The average total acceptance corrections varied between 30% and 50% including smearing of the distributions due to finite detector resolution and reconstruction inefficiencies determined from the data. The cross sections $d\sigma/d\log(x)$ and $d\sigma/dQ^2$ are shown in fig. 4. The $\log(x)$ representation was chosen in order to remove the trivial $1/x$ dependence of the cross section [eq. (3)]. The full error bars correspond to the statistical error which is the dominating uncertainty. The systematic errors are shown separately. All points are subject to a common additional uncertainty of 7% due to the luminosity measurement error. In the accessed kinematic range the measured deep inelastic cross section, not corrected for radiative effects, amounts to $\sigma = 92 \pm 11(\text{stat.}) \pm 12(\text{syst.})$ nb.

The calculation of the systematic uncertainty included the following error sources: possible shifts of the energy scale by 2% and of θ_e by 3 mrad; uncertainties in the trigger (2%) and detector (4%) efficiency calculations; electron and proton beam induced background (5%); photoproduction contamination in both the lowest x and Q^2 bin (15%); the influence

[#2] Note that the y_h–y_e cut was applied only for $y_e > 0.6$. Thus it served only to remove background in the lower part of the energy distribution and has no effect on the x, Q^2 distributions.

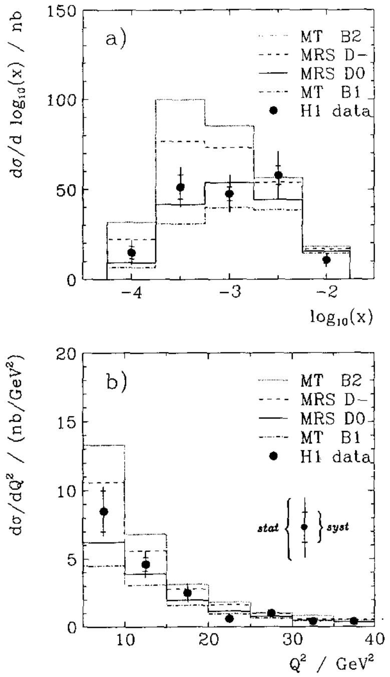

Fig. 4. Differential cross sections (a) $d\sigma/d\log_{10}(x)$ and (b) $d\sigma/dQ^2$ in the range $0.6 > y > 0.025$ and for $Q^2 > 5$ GeV^2 and $\theta_e < 174°$. The full lines show the results of the cross section calculations [13,14] for different parton density parametrizations. The cross sections are not corrected for radiative effects. The full error bars correspond to the statistical errors; the smaller systematic errors are also indicated.

of different structure functions and hadronization uncertainties on the acceptance calculation (12% at low x) and the bin size correction (5%); the statistical error of the Monte Carlo calculation at the largest Q^2 (5% at most).

Fig. 4 shows calculations of the cross section for the quark-distribution parametrizations MTB1, MTB2 [18] [#3] and MRSD0, MRSD− [15], using the program [13,14]. Note that the parametrizations [15] were obtained from data including the recent NMC measurements [3] which extend to $x = 0.008$ at $Q^2 = 4$ GeV^2. The parametrizations differ in their assumptions on the extrapolation of the quark and gluon densities at lower x. Neither data nor firm theoretical predictions [19] are available in this kinematic region. The MTB2 and MRSD− distributions assume a rapid growth of the parton densities with decreasing x, while MTB1 and MRSD0 assume a more moderate growth. In the kinematic range of our measurements the cross sections are 153 and 128 nb for MTB2 and MRSD− and 69 and 88 nb for MTB1 and MRSD0, respectively. Using the program [13,14] we assumed R to be zero, eq. (3). This leads to an overestimation of the theoretical cross section values by not more than 2% if $R = 0$ is replaced by the leading order QCD expression for R. The model calculations agree within two standard deviations with our measurement, except for that made with MTB2, which is more than three standard deviations larger.

The theoretical calculations include the contribution of higher order radiative corrections which have not been subtracted from the data. The corrections were calculated [17] in the measured region and are expected to change the cross sections by about 40% at the lowest x and Q^2 values. They are an order of magnitude smaller at the largest x and Q^2 values. The derivation of the Born cross sections, and of F_2, from the measured cross sections requires an iterative procedure, which is left to future analyses with higher statistics.

6. Conclusions

Deep inelastic scattering has been observed for the first time in a kinematic region that extends down to $x = 10^{-4}$ for Q^2 above 5 GeV^2. The data presented here stem from the first luminosity period at HERA, with collisions of 26.7 GeV electrons on 820 GeV protons. The spectrum of the scattered electron energy has been measured down to $E'_e = 6$ GeV. It exhibits the predicted peak around the electron beam energy and is rather flat at smaller energies. The simultaneous measurement of the inclusive reaction kinematics using the scattered lepton and the hadronic energy and angles has been shown to be an effective means of reducing the large photoproduction background at low scattered electron energies. This also extends the range of y which can be accurately measured to lower y. A measurement of the x and the Q^2 dependent cross sections in the range $Q^2 > 5$ GeV^2, $0.6 > y > 0.025$ and $\theta_e < 174°$ gives $\sigma = 92 \pm 11$(stat.) $\pm$ 12(syst.) nb.

[#3] The parton density parametrizations in the DIS scheme were used.

Acknowledgement

We are grateful to the HERA machine group whose outstanding efforts made this experiment possible. We appreciate the immense effort of the engineers and technicians who constructed and maintained the detector. We thank the funding agencies for financial support. We acknowledge the support of the DESY computer center. The non-DESY members of the Collaboration also wish to thank the DESY directorate for the hospitality extended to them.

References

[1] M. Breidenbach et al., Phys. Rev. Lett. 23 (1969) 935.
[2] J. Feltesse, Proc. Lepton photon Conf. (SLAC, Stanford, CA, 1989), ed. M. Riordan (1989) p. 13, and references therein.
[3] New Muon Collab., P. Amaudruz et al., CERN preprint PPE-92-124, Phys. Lett. B, to appear.
[4] F. Eisele, First results from the H1 experiment at HERA, in: Proc. 26th Intern. Conf. on High energy physics (Dallas, TX, 1992), to appear, and DESY preprint 92-140 (1992);
F. Brasse, The H1 detector at HERA, in: Proc. 26th Intern. Conf. on High energy physics (Dallas, TX, 1992), to appear, and DESY preprint 92-140 (1992).
[5] H1 Collab., The H1 detector at HERA, Nucl. Instrum. Methods, to be submitted.
[6] B. Löhr, First results from the ZEUS experiment at HERA, in: Proc. 26th Intern. Conf. on High energy physics (Dallas, 1992), to appear.
[7] A. Blondel and F. Jacquet, Proc. An *ep* facility for Europe, ed. U. Amaldi, DESY report 79/48 (1979) p. 391.
[8] H1 Collab., T. Ahmed et al., Phys. Lett. B 299 (1993) 374.
[9] H1 Collab., The backward electromagnetic calorimeter in H1, Nucl. Instrum. Methods, to be submitted.
[10] H1 Collab., T. Ahmed et al., Phys. Lett. B 298 (1993) 469.
[11] H1 interface program to LUCVDM of the LUCIFER package of G. Ingelman and A. Weigend (see DESY preprint 87-018), Comput. Phys. Commun. 46 (1987) 241.
[12] T. Sjöstrand, PYTHIA at HERA, Proc. Workshop on Physics at HERA (Hamburg), eds. W. Buchmüller and G. Ingelman, Vol. 3 (1991) p. 1405.
[13] A. Kwiatkowski, H. Spiesberger and H.-J. Möhring, Comput. Phys. Commun. 69 (1992) 155, and references therein.
[14] G. Ingelman, program manual LEPTO 5.2, unpublished;
H. Bengtsson, G. Ingelman and T. Sjöstrand, Nucl. Phys. B 301 (1988) 554.
[15] A.D. Martin, W.J. Stirling and R.G. Roberts, Durham preprint DTP-92-16 (1992).
[16] H. Spiesberger et al., Proc. Workshop on Physics at HERA (Hamburg), eds. W. Buchmüller and G. Ingelman, Vol. 3 (1991) p. 798.
[17] A. Akhundov et al., Proc. Workshop on Physics at HERA (Hamburg), eds. W. Buchmüller and G. Ingelman, Vol. 3 (1991) p. 1285;
A. Akhundov et al., private communication.
[18] J. Morfin and W.K. Tung, Z. Phys. C 52 (1991) 13.
[19] L.V. Gribov, E.M. Levin and M.G. Ryskin, Nucl. Phys. B 188 (1981) 555; Phys. Rep. 100 (1983) 1;
A.H. Mueller and J. Qiu, Nucl. Phys. B 268 (1986) 427.